nature communications



Article

https://doi.org/10.1038/s41467-025-64416-9

Status dystonicus is a distinct state characterized by pallidal beta-band activity

Received: 30 January 2025

Accepted: 12 September 2025

Published online: 22 October 2025



Arjun Balachandar ® ^{1,2,3,4,5}, Lindsey M. Vogt ® ¹, Karim Mithani¹, Sebastian C. Coleman¹, Mark Ebden ® ¹, Andrea Leblanc-Miller¹, Sara Breitbart¹, Alfonso Fasano ® ^{2,3,4,6,7}, Carolina Gorodetsky ® ¹ ⊠ & George M. Ibrahim ® ¹ ⊠

Status dystonicus (SD) is a poorly known neurological emergency requiring urgent interventions, including deep brain stimulation (DBS) targeting the globus pallidus interna (GPi). The sensing capabilities of DBS electrodes provide an opportunity to study the pathophysiology of SD. Here, we study local field potentials (LFPs) from GPi-DBS electrodes implanted in a cohort of 10 children longitudinally during SD, recovery and relapse (recording range 11-1155 days). During SD, we report an increase in the periodic component of the power spectrum within the beta-band along with increases in burst amplitude compared to recordings in non-SD states. Furthermore, relapsed SD is characterized by a return of excessive beta signatures. Beta-specific LFP power is also significantly associated with worse quality-of-life scores (PedsQL, $R^2 = 0.695$). We identify circadian pallidal beta-band periodicity in one participant with chronic narrowband beta-power recordings over months, with significant increase in power during SD. These rare recordings in children with SD point to excessive pallidal beta-band activity as a biomarker of SD. Our findings further suggest that SD is a distinct state with important implications for understanding dystonia pathophysiology, tracking dystonia states from intracranial activity and potential adaptive DBS treatments.

Dystonia is a hyperkinetic movement disorder that presents with sustained or intermittent muscle contractions leading to repetitive twisting movements and/or abnormal postures¹. Dystonia can be focal (limited to one body part), segmental (affecting two or more adjacent body parts) or generalized (involving most of the body), and ranges in severity from mild to life-threatening. Status dystonicus (SD) is poorly understood and represents the most severe form of dystonia, predominantly affecting children^{2,3}. Refractory SD^{4,5}, which persists despite pharmacotherapy, can result in life-threatening consequences

including metabolic derangement, respiratory/bulbar dysfunction, pain and fractures 6 , with mortality rates between $10-12.5\%^{4.7}$.

Deep brain stimulation (DBS) of the globus pallidus interna (GPi) is an effective and durable treatment for refractory SD^{5,8} that improves survival and reverses refractory SD in over 90% of participants⁸⁻¹⁰. It is generally safe and has been performed in children as young as 2 years of age^{2,8}. Early implantation and initiation of stimulation as an emergency treatment for refractory SD⁸ is thought to be effective across both inherited and acquired aetiologies of dystonia^{8,10,11}.

¹Hospital for Sick Children, University of Toronto, Toronto, Ontario, Canada. ²Division of Neurology, University of Toronto, Toronto, Ontario, Canada. ³Edmond J. Safra Program in Parkinson's Disease and Morton and Gloria Shulman Movement Disorders Clinic, Toronto Western Hospital, UHN, Division of Neurology, University of Toronto, Toronto, Ontario, Canada. ⁴Krembil Research Institute, Toronto, Ontario, Canada. ⁵CenteR for Advancing Neurotechnological Innovation to Application (CRANIA), Toronto, Ontario, Canada. ⁶Department of Biomedical Sciences, Humanitas University, Via Rita Levi Montalcini 4, 20090 Pieve Emanuele, Milan, Italy. ⁷IRCCS Humanitas Research Hospital, via Manzoni 56, 20089 Rozzano Milan, Italy. ©e-mail: carolina.gorodetsky@sickkids.ca; george.ibrahim@sickkids.ca

The pathophysiology of SD is currently poorly understood, and there are no known markers that can identify transitions between a baseline dystonic state (i.e., non-SD) and SD. Dystonia is a network disorder linked to pathological signaling between sensorimotor cortices. the cerebellum and the basal ganglia¹²⁻¹⁵. The use of sensing-capable DBS devices in pediatric dystonia has recently provided a unique opportunity to investigate intracranial correlates of SD through local field potentials (LFPs) within the basal ganglia. Several oscillatory patterns within the basal ganglia have been shown to characterize aberrant subcortical networks linked to dystonia^{16,17}. In adults with focal dystonia, lowfrequency theta to alpha-band (4-12 Hz) LFP activity have been observed in the GPi and subthalamic nucleus (STN)¹⁵⁻²⁰. Faster oscillatory signatures have been identified across other movement disorders, including STN beta-band (13-30 Hz) activity in Parkinson's disease (PD)²¹⁻²³. The substrates of the frequency-specific oscillatory activity are thought to be bursting activity in the basal ganglia, which has been reported in adults with dystonia and PD^{20,23-28}. In addition, non-oscillatory or aperiodic components of the power spectrum have also been thought to characterize states of altered balance of inhibition and excitation in movement disorders²⁸⁻³². To date, the oscillatory and non-oscillatory electrophysiological signatures of SD remain elusive.

Multi-scale dynamic changes in power spectral density (PSD) estimates may also characterize pediatric dystonic states. Clinical improvements in dystonia are often associated with sleep and/or sedation^{4,5,7,33} and circadian patterns have been previously reported in other movement disorders^{34–36}, with pallidal beta-band power usually decreasing at night in PD³⁷. Circadian periodicity gleaned through analysis of LFP activity has also been correlated to risk of worsening of other neurological disorders, including epilepsy³⁸ and neuropsychiatric disorders³⁹. The multi-scale dynamics of LFPs in SD are unknown, and although implanted devices are equipped with chronic narrowband sensing capabilities, they have yet to be leveraged to predict the risk of transition to SD states.

Biomarkers to identify transition into SD are particularly critical since children at risk often have chronic baseline dystonia outside of the SD state, which may be difficult to differentiate^{4,5,7}. Indeed, children with SD often experience relapses that can be difficult to identify at the onset, but which necessitate urgent and significant increases in acute management^{4,5,7}. In addition to tracking of dystonia states, intracranial biomarkers may inform the development of closed-loop adaptive DBS (aDBS) algorithms that selectively modulate stimulation during such pathological states, providing optimal stimulation when required and reduced side effects and battery usage when not needed^{40–42} as previously studied in PD^{40–42} and adult dystonia²⁴. The identification of SD-specific intracranial biomarkers and their multi-scale dynamics^{43,44} are therefore a necessary step before aDBS can be successfully implemented for SD.

Our objective in this study was to identify intracranial neural biomarkers of SD. We prospectively collected LFP timeseries longitudinally across months-to-years in a unique and rare cohort of 10 pediatric dystonia participants implanted with sensing-capable GPi DBS for SD. In tandem, we collected detailed clinical outcome measures pertaining to dystonia severity and health-related quality of life (HRQoL) at predefined timepoints through the Child & Youth Comprehensive Longitudinal Database for Deep Brain Stimulation (CHILD-DBS)⁴⁵. We sought to characterize GPi LFPs during SD and non-SD states based on oscillatory (periodic) and aperiodic components of the power spectrum, correlating them with HRQoL and dystonia severity. We leveraged the long-term narrowband recording capability of the DBS system to monitor betaband power in one participant to GPi-circadian patterns rhythms in SD. Finally, as a proof-of-concept towards future applications in aDBS, we trained machine learning classifiers to predict dystonia states using LFP data as features. Collectively, these analyses provide a demonstration of GPi-LFPs across SD, recovery, and relapse, presenting avenues to monitor and intervene in this rare life-threatening condition.

Results

Data were analyzed from a rare cohort of ten children with refractory SD who met surgical criteria for DBS and underwent bilateral implantation of the GPi with the Medtronic Percept PC neurostimulator attached to DBS leads bilaterally (lead localization shown⁴⁶ in Fig. 1A). Six male and four female participants were included, with an average age at surgery of 7.8 ± 3.6 (mea $n \pm$ std) years. The phenomenology of the dystonia was tonic (i.e., more fixed) in two participants and phasic (i.e., more mobile) in eight participants^{47,48}.

All participants except one experienced clinical improvement with eventual resolution of SD after DBS and eventual discharge from hospital (DBS programming settings listed in Supplementary Table 1). Dystonia severity was measured using the movement subscale of the Burke–Fahn–Marsden Dystonia Rating Scale (BFMDRS)⁴⁹. The normalized BFMDRS (BFMDRS_{normalized}) decreased significantly from the SD period (0.98 \pm 0.03) to the non-SD period (0.64 \pm 0.28) across all participants (U = 67, p = 0.008). All but one participant with long-term follow-up experienced a Minimal Clinically Important Difference (MCID)⁵⁰ of the BFMDRS (>0.17 decrease in BFMDRS_{normalized}). Most participants had a single SD episode; however, three participants experienced multiple relapse episodes of SD.

Neural activity was recorded as LFP time series data longitudinally during SD in all participants and additionally non-SD in seven participants over the course of 11 to 1155 days (median: 183 days). Three participants only had recordings in the SD state due to death (n=1) or hardware replacement/removal (n=2). A total of 183 time series recordings (118 ± 103 seconds duration) were obtained across all participants (18.3 ± 12.2 recordings per participant). Table 1 details the clinical characteristics of the cohort including dystonia etiology and neuroimaging, while Table 2 shows the LFP recording metrics and concurrent medications used.

GPi beta-band oscillatory activity was increased during SD

Timeseries obtained with the Percept PC device from each recording session were converted to the frequency domain and normalized to facilitate comparisons between dystonia states (SD vs. non-SD) within and across participants (Fig. 1). We identified a prominent beta-band peak (between 12.5-30 Hz) during SD, seen both cumulatively across all participants (Fig. 1B) and in individual participants (Supplementary Fig. 1). Participants experiencing multiple SD events showed recurrence of the beta peak during subsequent SD recordings (sample participant shown in Fig. 1C). The beta band-limited power was significantly higher during SD (0.261 ± 0.147) compared to non-SD (0.134 ± 0.084; U = 6175, $p_{corrected}$ < 0.001) across all recordings from all ten participants (Fig. 2B), and increased individually in all but two participants (Table 3). This finding was robust when accounting for variability across recurrent SD episodes and multiple participants (β = 0.166; p < 0.001).

To test whether the increased beta-band power was driven by periodic or aperiodic components of the PSD, we applied the Fitting Oscillations & One Over f (FOOOF) algorithm as shown for an illustrative participant in Fig. 2A. This analysis showed that the peak power of the periodic component of the PSD in the beta-band significantly increased during SD (0.653 ± 0.325 vs. 0.511 ± 0.230 ; U=4208, $p_{corrected}=0.007$) across all recordings and participants (Fig. 2B) and in individual participants (Table 3). This result was valid when controlling for recurrent SD episodes and multiple participants ($\beta=0.166$; p<0.001). The peak frequency within the beta band was slightly higher in SD (23.39 ± 13.04 vs. 19.45 ± 15.24 ; U=4370, $p_{corrected}=0.002$).

Periodic peak power was not associated with participantspecific factors

The beta-band peak power was only affected by the dystonia state (SD vs. non-SD; β = 0.157; p < 0.001) and not associated with participant-specific factors, including age (β = -0.009; p = 0.602), sex (β = -0.105; p = 0.450), phenomenology (phasic vs. tonic, β = -0.196; p = 0.235) or

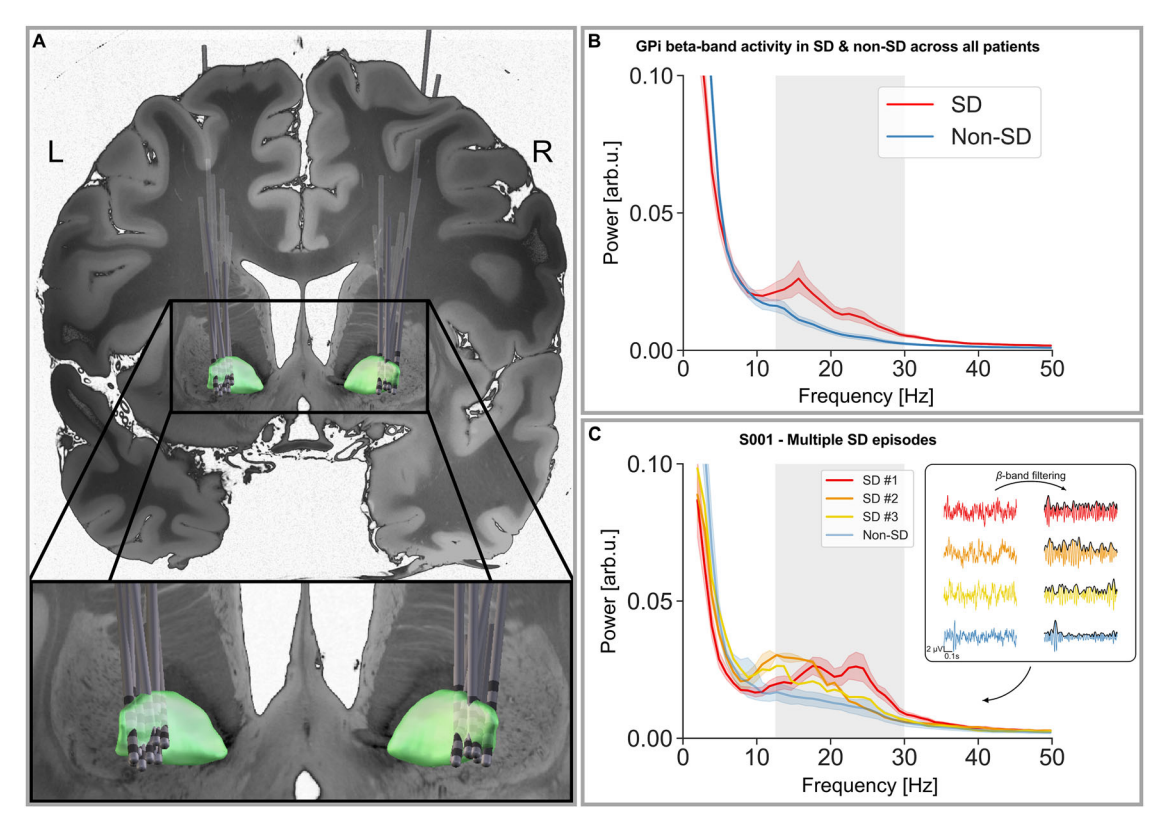


Fig. 1 | **GPi activity during status dystonicus.** A DBS leads across all ten participants were localized to the GPi (shown in green) in normalized atlas space (MNII52) using the DISTAL atlas. Figures B-C illustrate power spectral density (PSD) plots, with the beta-band (13-30 Hz) shown in grey shaded regions. **B** An aggregate PSD plot across all LFP recordings from all participants showed excessive activity during SD (red) compared to non-SD (blue). **C** Participant S001 was among those who experienced multiple SD episodes (colored lines), experiencing three discrete SD

episodes each with increased beta-band activity as seen in the respective PSD plots (left). Raw LFP time series traces and corresponding filtered beta-band activity with Hilbert envelopes are also shown for each dystonia state (right). In all line plots, the dark lines represent the mean power and the shaded regions indicate the 95% confidence intervals. Arb.u. arbitrary units, GPi globus pallidus interna, SD status dystonicus.

etiology (inherited vs. acquired, β = -0.018; p = 0.895). Moreover, there was no effect of concurrent exposure to sedating medications at the time of recording on peak power, including benzodiazepines (β = 0.063; p = 0.452), non-benzodiazepine (clonidine, chloral hydrate or baclofen) medications (β = 0.163; p = 0.198), or any sedating medications (benzodiazepine or non-benzodiazepine) in general (β = 0.153; p = 0.108). Benzodiazepine dosage also did not affect peak power (β = 0.255; p = 0.120). Hence, elevated beta-band oscillatory activity distinguished SD independent of participant factors.

Beta-band bursting amplitude and burst amplitude-duration relation increased in SD

The increased pallidal beta-band oscillatory activity characterizing SD was driven by beta-band bursting activity. Across 23,667 detected bursts (7927 bursts in SD, 15,740 in non-SD), the mean bursting amplitude significantly increased during SD (0.90 \pm 0.32) compared to non-SD (0.62 \pm 0.25; U = 649412, p < 0.001) (Fig. 3A&B). There were no differences in the mean bursting rate (bursts/min) (65.15 \pm 10.31 vs.63.88 \pm 10.73; U = 439655, p = 0.766), or in the mean burst duration (0.22 \pm 0.05 sec vs. 0.22 \pm 0.05 sec; U = 438744, p = 0.826) (Fig. 3B).

We examined the relationship between burst amplitude and duration to investigate the dynamics of neuronal synchronization in the GPi (Fig. 3C). Burst amplitude was correlated to burst duration in both states (SD: β =1.754; p<0.001, non-SD: β =1.270; p<0.001). Notably, SD was characterized by significantly higher amplitudes for a given duration as this state had a significant modifying effect on the amplitude-duration relationship (β =0.484; p<0.001). Additionally, bursts in SD had a higher baseline amplitude (adjusted intercept:

 β = 0.489 vs. β = 0.35; p < 0.001). This stronger amplitude-duration relationship further supported the observation that SD is a state with pallidal bursting activity of similar durations, but elevated amplitudes compared to non-SD.

GPi aperiodic activity was decreased in SD

Unlike period beta activity, non-oscillatory (aperiodic) activity was significantly decreased during SD compared to non-SD (Fig. 2C). The aperiodic offset significantly decreased during SD (-0.451 ± 0.330 vs. -0.166 ± 0.262 ; U=1549, p<0.001) across all recordings and participants using the FOOOF algorithm⁵¹, corresponding to a decreased intercept of non-oscillatory background activity. Similarly, the aperiodic exponent of the 1/f-shape background activity also significantly decreased in SD (1.445 ± 0.385 vs. 1.839 ± 0.399 ; U=1558, p<0.001), indicating a flatter slope of the background activity. The effects of dystonia state remained significant on both aperiodic offset ($\beta=-0.218$; p<0.001) and exponent ($\beta=-0.221$; p=0.001) respectively across recurrent SD episodes.

GPi beta-band activity correlated with worsened quality of life

By leveraging prospectively collected data through the CHILD-DBS longitudinal registry⁴⁵, we found that band-limited beta-band power was significantly associated with the Pediatric Quality of Life Inventory (PedsQL), a validated parental reported outcome (PRO)^{52–54} (Fig. 4A, p=0.03; $\beta=-92.7$, $R^2=0.695$). Dystonia state was neither associated with (p=0.746; $\beta=14.9$) nor modified (p=0.864; $\beta=-11.6$) the association between beta power and PedsQL. The association was beta-band specific as there was no association between PedsQL and activity

characteristics
Ĕ
clinic
and
demographics
Participant c
=
rable

Q	Dystonia Phenomenology	Dystonia Etiology	Sex	Age at DBS (range in years)	Years followed post- DBS	MRI Abnormalities	# Clinical assessments	BFMDRS-M: SD (range)	BFMDRS-M: Non- SD (range)
S001	Tonic	HIE/Kernicterus, Negative Genetic Workup	ш	10–15	3.5	Atrophy, T2 hyperintense lesions in periacqueductal grey and right thalamus, globus pallidus	5	97	49.5-118
8002	Phasic	Suspected Genetic, Negative Workup	Σ	10–15	က	Reported normal	2	114.5	43.5-69.5
8003	Tonic	SCN2A Encephalopathy	LL.	<5	2	Progressive volume loss, T2 hyperintensitiy in periventricular/deep white matter	3	86	58-60
S004	Phasic	Progressive AFG3L2- related dyskinesia	LL.	<5	1.5	Thinning of corpus callosum, progressive volume loss	1	37-45.5	13
S005	Tonic	MECP2 - Rett Syndrome	ш	5-10	1	Volume loss	3		69-72.5
900s	Tonic	PKAN (progressive)	Σ	<5	1	Eye of the tiger, PKAN - related changes	2	83	
2005	Tonic	HIE secondary to DKA	Σ	15–20	1.5	Cystic encephalomalacia in globus pallidus and striatum	1	83	48.5-91
8008	Tonic	Prematurity/Perinatal Brain Injury	Σ	10–15	3	Diffuse volume loss	1	65-108	37
6008	Tonic	Perinatal Brain Injury, Negative Genetic Workup	Σ	10–15	1 mo	Corpus callosum thinning, volume loss	1	85-88	-
S010	Tonic	Perinatal Brain Injury, Negative Genetic Workup	Σ	10–15	е то	T2 hyperintensity in bilateral caudate and putamen	2	82.5	72-86

AFG312 AFG3 ATPase family gene 3-like 2, BFMDRS-M Burke-Fahn-Marsden Dystonia Rating Scale movement subscale, DBS deep brain stimulation, DKA diabetic ketoacidosis, F Female, HIE hypoxic-ischemic encephalopathy, M Male, MECP2 methyl CpG binding protein 2, N No, PKAN Pantothenate kinase-associated neurodegeneration, SCN2A sodium voltage-gated channel alpha subunit 2, SD status dystonicus, Y Yes. at any other frequency band (Supplementary Fig. 2, alpha-band: p = 0.560; $\beta = 20.1$, theta-band: p = 0.358; $\beta = 51.6$). Averaging band-limited powers across both hemispheres again showed a beta-band specific association (p = 0.005; $\beta = -130.9$, $R^2 = 0.501$), with no such association observed for other frequency bands (alpha-band: p = 0.532; $\beta = 26.7$, theta-band: p = 0.132; $\beta = 137.4$).

Interestingly, we did not identify any significant association between BFMDRS ratings and PedsQL (p=0.355; $\beta=-0.435$). In turn, we also observed no relations between BFMDRS and activity in any frequency band, including the beta- (Fig. 4B, p=0.474; $\beta=-49.4$), alpha- (p=0.529; $\beta=-23.8$), and theta-bands (p=0.681; $\beta=20.2$). These null associations persisted when band-limited powers were averaged across hemispheres (beta-band: p=0.571; $\beta=-35.0$, alpha-band: p=0.941; $\beta=-3.9$, theta-band: p=0.716; $\beta=34.6$). This indicated that although the BFMDRS decreased in non-SD periods, it was neither associated with PedsQL nor changes in band-limited power.

GPi narrowband beta-band activity demonstrated similar circadian periodicity but altered power dynamics during SD

Given the attenuating effects of sleep patterns on dystonia and potentially SD, we next sought to study dynamic multiscale changes in the beta-band in one participant with chronic narrowband recordings (Fig. 5A) over the course of 91 days and 22 h (SD: 31 days, 6 h; Non-SD: 60 days, 16 h). We found that the beta-band LFP activity characterizing dystonia states was modulated by circadian rhythms, exhibiting strong circadian periodicity in both SD and non-SD but significantly higher beta-band powers during SD across both daytime (12:00 - 19:00) and nighttime (21:00 - 06:00), and treated with similar medications (diazepam, chloral hydrate, tetrabenazine, gabapentin and clonidine) at regular intervals throughout both dystonia states. First, the Rayleigh test confirmed significant circadian modulation of beta-band power in both SD (p < 0.001) and non-SD (p < 0.001), while a permutation-based Kuiper test revealed no significant difference in the 24-hour distribution shapes between the two conditions (V = 0.0239, p = 0.605). Next, applying a Linear Autoregressive (LAR) model³⁹ (Supplementary Fig. 3), we computed an overall R2 of 0.809 across the SD period and R2 of 0.865 across the non-SD period. The models showed circadian periodicity with a mix of recent lags (e.g. 10 min and 30 min prior respectively) and longer lags (e.g. 14hr10min and 18hr30min prior) for optimal prediction. There was no difference in the mean daily model fit between SD ($R^2 = 0.681$) and non-SD ($R^2 = 0.693$, t = -0.481, p = 0.632).

Assessment of beta-band power dynamics revealed that the mean power increased during daytime in both SD (3754 \pm 1397 vs. 2501 \pm 1355; U = 2078527, $p_{corrected}$ < 0.001) and non-SD (1213 \pm 579 vs. 951 \pm 450; U = 5892577, $p_{corrected}$ < 0.001). However, SD was characterized by greater power across daytime and nighttime (Fig. 5B, Daytime: U = 3748008, $p_{corrected}$ < 0.001; Nighttime: U = 5969144, $p_{corrected}$ < 0.001). Moreover, SD experienced a larger average proportional increase in daytime power (Fig. 5C, 0.31 \pm 0.27 vs. 0.21 \pm 0.20; U = 1355, $p_{corrected}$ = 0.007).

Machine learning models classified SD and non-SD states from LFP PSDs

As a proof-of-concept towards future aDBS paradigms for SD, we assessed if LFPs could be used as features to train ML models to classify the corresponding dystonia state (SD vs. non-SD). Random forest classifiers predicted dystonia state using LFPs with an Area Under the Receiver Operating Characteristics Curve (AUROC) of 0.76, using Leave-One-Patient-Out Cross-Validation (LOPOCV) where training in each fold occurred on nine patients' LFP data and tested on a holdout tenth patient (Supplementary Materials).

Discussion

Status dystonicus is a life-threatening condition with no known biomarkers to define transitions between baseline dystonic states and SD.

Table 2 | Participant electrophysiological recordings and medications

ID	# LFP time series recordings	DBS inserted during SD	Non-SD LFP recorded (reason if N)	# SD post DBS	Benzo - SD	Benzo - Non- SD	Non- benzo SD	Non-benzo Non-SD
S001	38	Υ	Υ	3	Υ	Υ	Υ	Υ
S002	22	N	Y	2	Υ	N	N	Υ
S003	23	Υ	Y	1	Υ	Υ	Y	N
S004	11	Υ	Y	1	Υ	Υ	Y	N
S005	15	Υ	Y	1	Y (PRN)	N	N	N
S006	27	Υ	Y	1	Υ	Υ	Υ	Υ
S007	37	Υ	Y	2	Υ	Υ	Y	N
S008	8	Υ	N (IPG switched to Medtronic Activa™)	0	Y	Y	Y	N/A
S009	2	Υ	N (Death due gastrointestinal inflammation)	0	Υ	N/A	Y	N/A
S010	10	Υ	N (DBS system explanted due to infection)	0	Υ	Y	Y	N

Benzo Benzodiazepine medication, DBS deep brain stimulation, LFP local field potential, N No, Non-benzo non-benzodiazepine medication (baclofen, chloral hydrate, clonidine), PRN pro re nata (i.e. medication taken as needed), SD status dystonicus. Y Yes.

In this study, we investigated neural activity from the GPi in a unique and rare cohort of children with SD and heterogeneous clinical features. We observed that excessive beta-band activity was a hallmark of SD, with 1) significantly increased periodic activity and bursting amplitude during SD, 2) significant correlations between beta-band power and HRQoL and 3) strong circadian periodicity and characteristic narrowband beta-band power increases during SD.

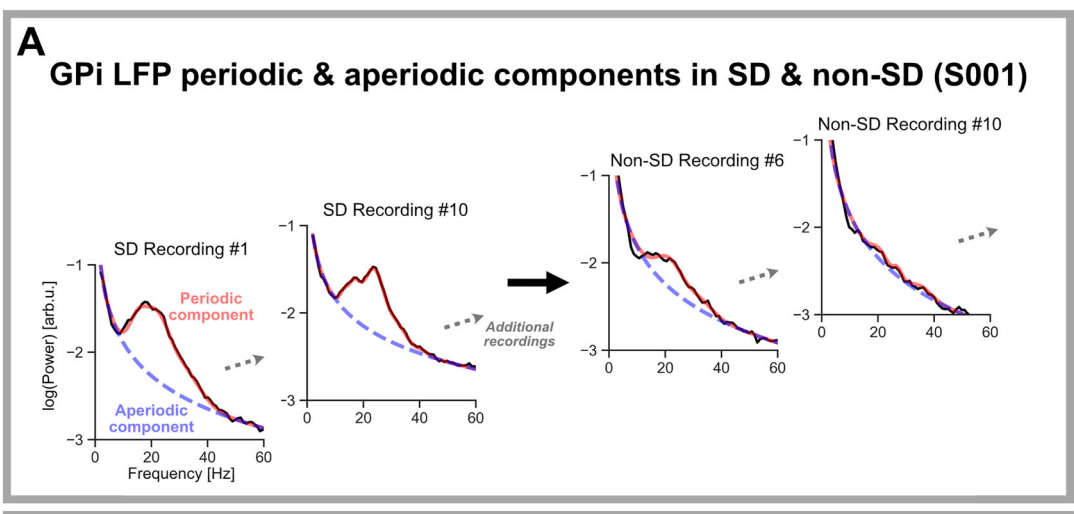
This study explores neurophysiological biomarkers of SD and involves a large cohort of pediatric participants with dystonia, using months-to-years of longitudinal LFP recordings. Although relatively rare and under-studied, GPi DBS is an increasingly recognized and utilized treatment for refractory SD⁸. Intracranial biomarkers are essential to track dystonia states and to differentiate SD episodes from chronic baseline levels of dystonia^{4,5,7}. Moreover, such markers are required for the development of aDBS targeted towards SD.

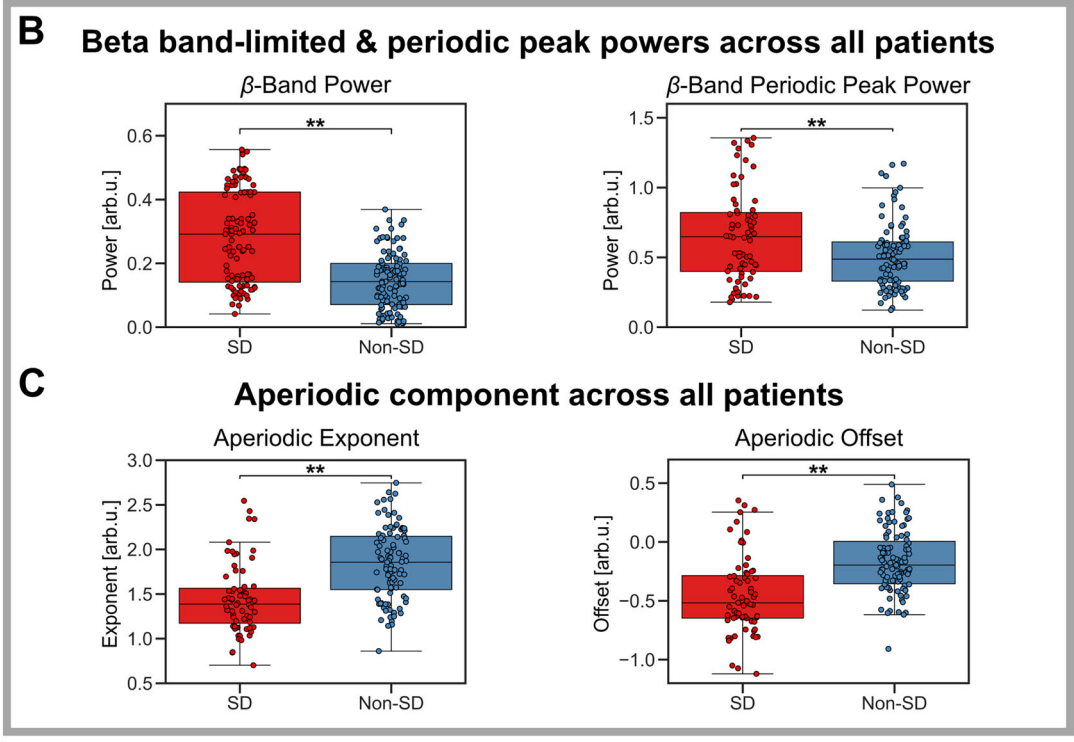
Our results demonstrate that increased pallidal beta-band activity is a hallmark of SD, characterized by an increase in the periodic component of the LFP. These findings suggest that SD is a measurable clinical state that is distinct from baseline dystonia. Prior studies have shown increases of low-frequency activity with dystonic symptoms^{16,17,55}. However, these were in adults with focal dystonia, and did not study the uniquely severe state of SD16,17,55. In prior case reports, our group has previously reported that GPi beta-band oscillatory peaks can be seen empirically in refractory pediatric SD^{56,57}. The current study represents a quantitative analysis of SD intracranial activity across multiple participants and LFP recordings. Importantly, our results provide evidence for the reproducibility of beta-band signatures as several participants experienced SD relapse and recurrence of high beta-activity states. These beta-band oscillations were only affected by dystonia state, and not associated with sedating medications (neither benzodiazepines nor non-benzodiazepines), etiology (inherited vs. acquired), sex or age, with patients ranging in age from early childhood at three to young adulthood at sixteen. Phenomenology (tonic vs. phasic) also did not modify beta-band activity at either the group or individual participant level. This supports the conclusion that highly excessive GPi beta-band activity is mechanistically involved in SD and may serve as a state-specific marker of SD independent of age or demographic factors, raising the possibility that our results may generalize beyond children.

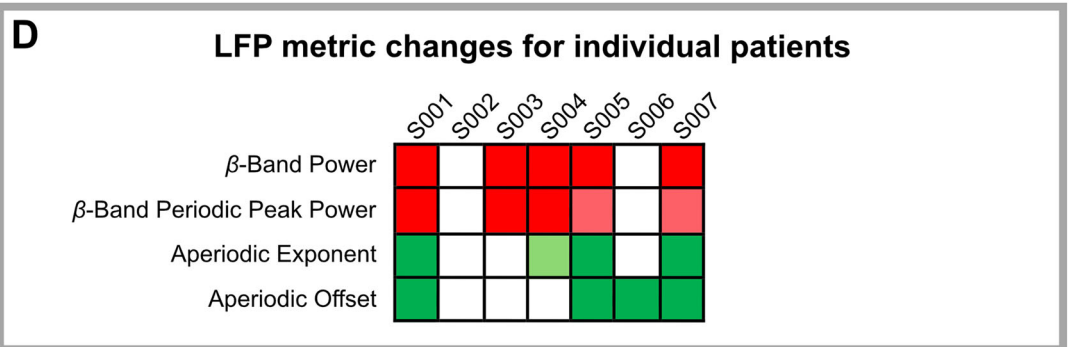
The current study presents an association between increased beta-band oscillatory activity in SD and GPi bursting activity, namely increased beta-band bursting amplitude without changes in duration. Bursting neurophysiology is of importance in movement disorders since excessive oscillatory activity may be partly explained by increased amplitude and/or duration of transient bursts of

synchronous activity^{25,58}, and may impair information transfer in the basal ganglia⁵⁹. Our results suggest that SD is a state associated with either larger numbers of synchronous pallidal neurons and/or increased neuronal firing intensity (i.e., increased bursting amplitude) 25, as opposed to progressive synchronization over time (i.e., increased bursting duration)^{25,60} or changes in phase. Bursting physiology in adults has been analogously described in PD, where increased beta-band bursting duration as opposed to amplitude may occur with worse motor symptoms^{20,25}, in contrast to our results in SD. However, bursting in dystonia has only been studied in small adult cohorts with primarily focal dystonia and not compared across different severities^{20,24,61}, making these distinct findings valuable to understanding the pathophysiology of SD.

Our study also identified that increased beta-band activity correlated significantly with lower HROoL as measured by the PedsOL, an association specific to the beta-band and present regardless of using band-limited powers from a single optimal hemisphere or averaged across both hemispheres. This relation was not modified by whether participants were in SD or non-SD states, demonstrating that excessive beta-band activity was a specific marker of worse HRQoL in dystonia. In children with chronic severe disorders like generalized dystonia, such HRQoL measures are critical clinical outcomes⁵²⁻⁵⁴. The PedsQL, a validated and widely-used pediatric HRQoL metric⁵², was chosen to be measured longitudinally in all DBS patients at our center through the CHILD-DBS registry⁴⁵ given its reliability⁵², construct validity across diverse populations^{53,54}, and sensitivity to meaningful changes⁵². This measure also captures important aspects of impairment observed during SD⁶. Intracranial correlates to such HRQoL measures are hence crucial as they are relevant to guiding management^{22,27}. It is interesting to speculate that the observed intracranial biomarkers in SD are superior to traditional clinical tools like the BFMDRS⁵⁷, a scale that while validated in adults^{49,50} has vet to be studied for validity and reliability in children^{62,63}. Of note, the LFP measures in our study did not correlate with BFMDRS, which itself was not correlated with HRQoL outcomes. This aligns with previous research indicating that the BFMDRS does not capture important HRQoL improvements post-DBS that can occur even without marked reductions in BFMDRS⁶⁴⁻ This limitation is particularly pertinent in children with DBS-responsive SD but persistent levels of baseline dystonia^{62,63}. For example, despite clinical improvement, some children experienced marginally decreased or increased BFMDRS scores during non-SD. The BFMDRS also poorly discriminates normal dystonic-like movements that are common in children^{62,67}, and is further difficult to apply in younger children such as some in our cohort⁶⁷. Our results underscore the major disadvantages of the BFMDRS in assessing clinical outcomes in







pediatric dystonia and support our focus on biomarkers of alternative validated measures of clinical severity, namely HRQoL, in this population.

We also analyzed the aperiodic component of LFPs and found that this non-oscillatory background activity was decreased during SD, supporting the findings that the increased beta-band activity in SD was primarily due to periodic oscillatory activity. Aperiodic activity itself, however, is also significant as it reflects the balance between inhibition and excitation across neuronal populations and may be lower in states of decreased inhibition^{28-31,68}. The aperiodic component in SD, characterized by a flatter 1/f spectral profile and lower intercept, may suggest an increase in pallidal excitatory background activity. This contrasts with the higher aperiodic activity observed in the less severe non-SD state, possibly representing increased inhibitory background

Fig. 2 | Beta-band periodic and aperiodic activity during status dystonicus.

A Periodic and aperiodic components of the LFP were computed for each recording across SD and non-SD, as shown for some recordings in exemplary participant S001. Dotted grey arrows indicate when numerous additional recordings (not shown) were obtained and analyzed similarly. **B** Band-limited beta-band power increased significantly ($p_{corrected} < 0.001$) in SD across all recordings from all participants (left; n = 183). This was explained by an increase in the periodic-component peak power ($p_{corrected} = 0.007$) across all participants/recordings (right; n = 183). **C** The non-oscillatory aperiodic activity increased in the non-SD period across all participants/recordings as represented by an increase in aperiodic exponent (left; $p_{corrected} < 0.001$, n = 183) and offset (right; $p_{corrected} < 0.001$, n = 183), further demonstrating that the increased beta-band activity in SD was due to oscillatory

activity. **D** Comparisons of SD to non-SD for each LFP metric are shown for each participant that had both SD and non-SD recordings. Red panels (dark red: p < 0.01; light red p < 0.05) represent statistically significant increases, green (dark green: p < 0.01; light green p < 0.05) significant decreases, and white no significant change in the corresponding metric during SD. All statistical comparisons were conducted with Mann-Whitney U-tests, Bonferroni-corrected for multiple comparisons. In all box-and-whisker plots shown, the center line of each box is the median, the box bounds represent the interquartile range (IQR) spanning from the first to third quartile, the whiskers extend to the furthest data points within 1.5 times the IQR from the edges of the box, while data points shown beyond the whiskers represent the outliers. Arb.u. arbitrary units, LFP local field potential, SD status dystonicus. **p < 0.01. *p < 0.05.

activity during clinical improvement. Studies post-DBS have also shown that STN aperiodic activity increases acutely with stimulation in adult dystonia³² and over months in PD independent of medication state and despite clinical stability²⁸, potentially suggesting increased inhibitory activity related to DBS and not related to clinical progression²⁸. Further investigations of dystonia-specific networks projecting to the GPi may elucidate the mechanisms of these pallidal aperiodic changes and clarify their role in SD pathophysiology.

We found that multi-scale patterns, namely circadian rhythms, further modulate the beta-band LFP activity characterizing dystonia states. Using continuous narrowband beta-band recordings over months, we showed strong circadian periodicity in both SD and non-SD but significantly higher power during SD across both daytime and nighttime. LFP circadian dynamics are a key consideration before they can be utilized effectively to track dystonia states longitudinally or employed as feedback markers in future adaptive DBS paradigms for SD^{43,44}. They are especially important in SD since clinical improvements are often associated with sleep and/or sedation^{5,33}, while sleep itself is disordered during SD⁵. Our findings that beta-band power increased during daytime in both SD and non-SD are analogous to prior studies showing that GPi beta-band power also usually increases during the day in adult dystonia³⁴ and PD³⁷. SD was further distinguished by elevated daytime beta-band power compared to non-SD, in keeping with our results from longitudinal time series recordings. The additional observation that beta-band power proportionately increased more during the day in SD raises the question if any corresponding relative worsening in clinical severity during the daytime is more pronounced than in non-SD. Furthermore, the increased nighttime beta-band activity in SD also prompts whether this is associated with the impaired sleep often seen during SD^{4,5,33}. Of note, this participant remained on similar sedating medications at regular intervals both during and post-SD, making an additional effect of increased sedation during SD or nighttime in general less likely to impact these findings. Although these results were derived from a single participant, they have not been previously studied in pediatric dystonia. This approach may inform future larger studies assessing chronic narrowband recordings in SD and non-SD pediatric dystonia to potentially allow continuous monitoring of neural correlates to clinical severity.

Lastly, we found that random forest classifiers could classify LFP PSDs based on dystonia state with moderate accuracy. Classifier performance was robust despite training using LOOPV to ensure that testing only occurred on unseen data from holdout patients, indicating that the PSD features defining dystonia states generalized across patients. ML models utilizing sensed LFP markers have been employed to classify neural states and guide aDBS in other movement disorders^{40,43,44,69}. Our proof-of-concept method may similarly inform the implementation of aDBS to treat SD in future studies with larger cohorts. Although there is a lack of evidence regarding recommended stimulation adjustments during SD beyond initial programming⁸, our institutional experience suggests a strategy of increasing stimulation frequency or amplitude during periods of dystonia exacerbation. The use of ML methods to classify neural states may not only allow for

adaptive stimulation changes but can also support timely optimization of urgent medical therapies and early hospital admission to monitor and manage potential complications proactively.

Several limitations warrant attention. Although SD is a rare condition and these recordings represent the largest dataset available in this exquisitely vulnerable and poorly understood population, this is a relatively small sample size limited by the sampling ability of the Percept device. We attempted to mitigate this by analyzing a large number of longitudinal time series recordings with heterogeneity in age, phenomenology, etiology, and medications. However, larger multicenter studies involving more participants, broader dystonia characteristics, and further cohort diversity to increase statistical power are needed. Quantifying SD-severity beyond SD versus non-SD may also help with further assessing the clinical heterogeneity of SD, which could provide a more nuanced understanding of beta-band activity in different types of refractory SD. Furthermore, LFP metrics were compared across dystonia states, including SD recurrences, and no clinical lesional effects were observed within one week post-operatively. However, a lesional effect potentially contributing to the findings cannot be ruled out, given the relatively small number of participants experiencing multiple SD episodes. Another limitation is that only one participant studied had chronic beta-band narrowband recordings. Future studies with more narrowband recordings across more participants, along with frequent standardized dystonia and sleep state assessments, could provide further insights into the relationship between LFP dynamics and clinical states. Additionally, although we localized all recording contacts to the GPi, directional sensing from the segmented DBS leads implanted in all patients was not utilized in this study but may have allowed further refinements in anatomical localization of pathological LFP activity. Lastly, the inherent limitations of the BFMDRS in pediatric populations and its lack of correlation with HRQoL outcomes underscore the need for alternative measures better representative of meaningful clinical changes, as neural activity may better correlate with such metrics.

In conclusion, our results show that excessive beta-band activity in the GPi is a biomarker of SD. These findings may inform larger studies, allowing the tracking of dystonia states from intracranial activity and future potential applications of adaptive DBS for severe dystonia.

Methods

Study design and participants

The study and all procedures were approved by the Research Ethics Board (REB) at HSC, and LFP and clinical data were collected through the CHILD-DBS registry⁴⁵. Written informed consent was obtained from all participants' families. In this prospective study, ten pediatric participants with a diagnosis of medically refractory SD underwent bilateral GPi DBS implantation at the Hospital for Sick Children (HSC) in Toronto, Canada, from January 2021 to Dec 2023. The inclusion criteria were individuals diagnosed with refractory SD by a neurologist and who received GPi DBS, either implanted for treatment of SD or who developed SD at some point after implantation. SD was defined as

metrics
potential
field
local
participant
Individual
Table 3

□	Beta-band band-limited power	imited power		Beta-band periodic	peak power		Aperiodic offset			Aperiodic exponent	1	
	SD (mean± standard deviation)	Non-SD (mean± standard deviation)	p (U- value)	SD (mean± standard deviation)	Non-SD (mean ± standard deviation)	p (U-value)	SD (mean ± standard deviation)	Non-SD (mean± standard deviation)	p (U-value)	SD (mean ± standard deviation)	Non-SD (mean± standard deviation)	p (U-value)
8001	0.358 ± 0.109	0.220 ± 0.080	0.010 (260)	0.606±0.226	0.373±0.167	0.003 (251)	-0.721±0.166	-0.508±0.173	<0.001 (42)	1.118±0.164	1.305 ± 0.215	0.007 (70)
8002	0.290±0.160	0.188±0.063	0.712 (41)	0.494±0.346	0.438 ± 0.288	0.967 (35)	-0.368±0.153	-0.260 ± 0.208	0.342 (24)	1.457±0.109	1.564 ± 0.379	0.967 (35)
8003	0.217±0.089	0.132 ± 0.030	0.006 (107)	0.710 ± 0.135	0.553±0.034	0.004 (72)	0.155±0.136	0.257 ± 0.120	0.203 (25)	2.151±0.237	2.236±0.176	0.314 (28)
8004	0.484±0.096	0.225 ± 0.062	0.009 (29)	1.258±0.105	0.729 ± 0.133	0.004 (30)	-0.395±0.177	-0.078±0.077	0.004 (2)	1.747 ± 0.149	1.904±0.077	0.052 (4)
2002	0.355±0.096	0.103±0.071	<0.001 (230)	0.917 ± 0.336	0.631±0.238	0.032 (174)	-0.637±0.143	-0.151 ± 0.213	<0.001 (2)	1.280 ± 0.166	1.973±0.338	<0.001 (3)
9008	0.081±0.035	0.046±0.018	0.072 (44)	0.386±0.150	0.316±0.145	0.335 (37)	-0.394±0.101	-0.285±0.137	0.072 (12)	1.445 ± 0.069	1.727 ± 0.161	<0.001 (1)
2002	0.137 ± 0.038	0.061±0.041	0.009 (135)	0.489 ± 0.147	0.356±0.171	0.039 (37)	-0.355±0.174	-0.027±0.170	<0.001(9)	1.474±0.133	2.117±0.191	<0.001 (3)
8008	0.083 ±0.030	N/A	N/A	0.453 ± 0.187	N/A	N/A	-0.608±0.086	N/A	N/A	1.371±0.115	N/A	N/A
8008	0.236±0.112	N/A	N/A	0.749 ± 0.097	N/A	N/A	-0.068 ± 0.163	N/A	N/A	1.854 ± 0.256	N/A	N/A
2010	0.146 ± 0.062	N/A	N/A	0.413 ± 0.194	N/A	N/A	-0.244 ± 0.155	N/A	N/A	1.607 ± 0.204	N/A	N/A
N/A no	t available, SD status dy	N/A not available, SD status dystonicus. Mann-Whitney U-tests were used for all comparisor	U-tests were	used for all comparisor	ins. p-values < 0.05 are bolded.	olded.						

a movement disorder emergency characterized by severe episodes of generalized or focal hyperkinetic movement disorders that had necessitated urgent hospital admission because of life-threatening complications regardless of the patient's neurological condition at baseline^{6,70}. Life-threatening complications included severe generalized dystonia itself, or associated complications of bulbar weakness. compromised upper airway patency, exhaustion/pain, metabolic imbalances, organ failure (e.g. respiratory, cardiac, renal), aspiration, rhabdomyolysis or failure to thrive⁷⁰. Refractory SD was defined as having failed all attempted in-hospital pharmacological/medical therapy, with ongoing severe dystonia and consequent complications^{5,8}. The criteria for surgical implantation were patients with refractory SD, which was defined as having failed all attempted in-hospital pharmacological/medical therapy, with ongoing severe dystonia and consequent complications8. The SD period was defined as beginning with the onset of SD hospital admission and ending with discharge. Participants and their families were not compensated for any research activities.

Participants had LFP recordings and clinical assessments longitudinally during SD in seven participants (S001–S007). Recordings and clinical assessments were conducted in SD-alone (S008–S010) in three participants who did not have recordings in the non-SD state. All subjects were programmed according to established guidelines⁸.

DBS surgery

DBS leads carrying 8 contacts for directional stimulation (SenSight model, Medtronic – Dublin, IR) with 1.5-mm spacing were placed bilaterally in the GPi. Direct targeting with pre-operative magnetic resonance imaging (MRI) was used. Surgical targeting was done as per HSC institutional approach. The two leads were connected using extensions tunneled to a Percept PC implantable pulse generator (IPG) implanted in the chest wall. No participants received IPG implantation in the abdominal wall.

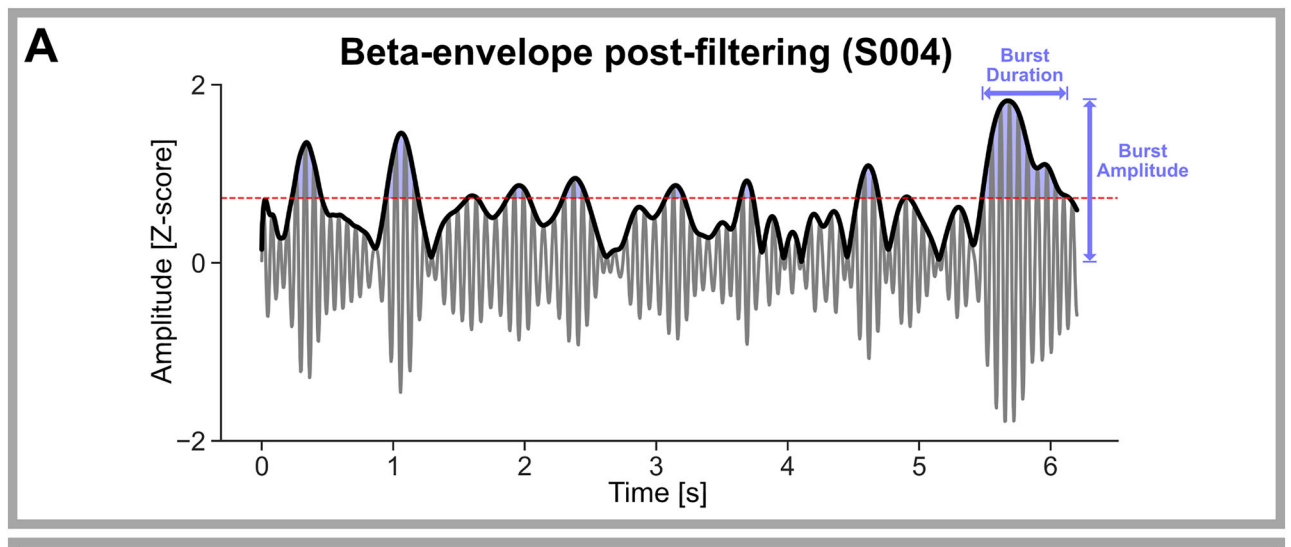
DBS electrode localization

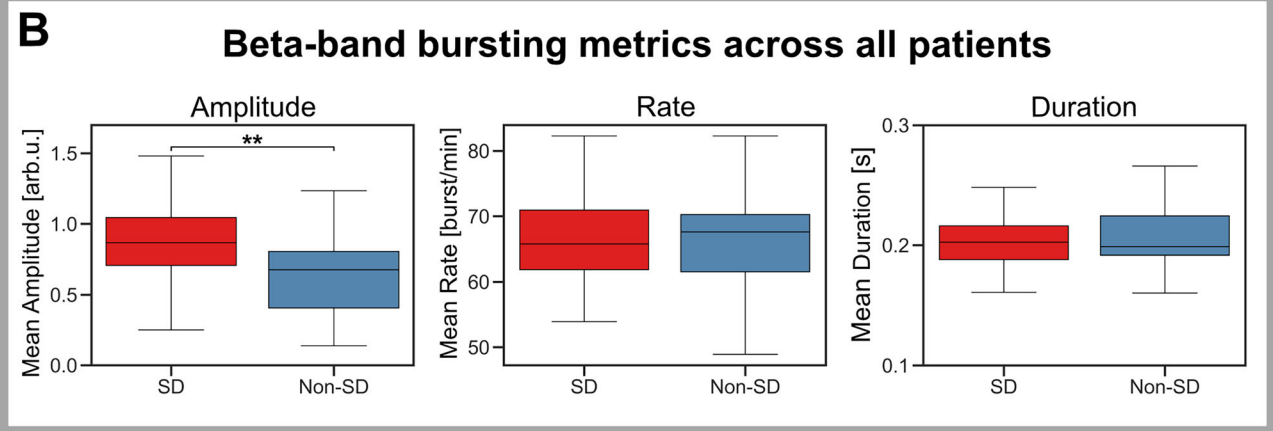
For each participant, pre- and post-operative high-resolution T1-weighted MRI sequences were obtained. Electrode reconstruction was conducted using the advanced processing pipeline in Lead-DBS⁴⁶ (version 2.5; https://www.lead-dbs.org/). Anatomical localization of implanted leads was conducted for all ten participants in normalized atlas space (MNI152). Three-dimensional reconstruction of the leads was illustrated on a 100-micron resolution, 7.0 Tesla FLASH brain. Due to anatomical differences between the adult and pediatric brains, although some leads appeared slightly off-target during localization (Fig. 1A), all the leads were confirmed to be anatomically well-positioned on pre-surgical planning and post-operative MRI (Supplementary Fig. 4).

Clinical assessments

Neurological examinations were conducted during SD as well as longitudinally for a subset of participants variably at 6 months, 1 year, 2 years, and 3 years after initial DBS surgery. The Burke–Fahn–Marsden Dystonia Rating Scale movement subscale (BFMDRS) measured dystonia severity at each time point that a given participant was assessed and was scored by a movement disorders neurologist. The BFMDRS_{normalized} was calculated individually for each participant by dividing the subsequent non-SD BFMDRS values by the preceding BFMDRS in SD. If the BFMDRS in the non-SD period decreased more than 17%, this was defined as a clinically-relevant Minimal Clinically Important Difference (MCID)⁵⁰. The mean of BFMDRS_{normalized} during SD and non-SD was compared across all participants.

HRQoL metrics were also measured longitudinally. The PedsQL is a validated PRO⁵² with good reliability and construct validity in a wide variety of general⁵³ and disease-specific⁵⁴ populations and with responsiveness to meaningful change⁵². The PedsQL was calculated





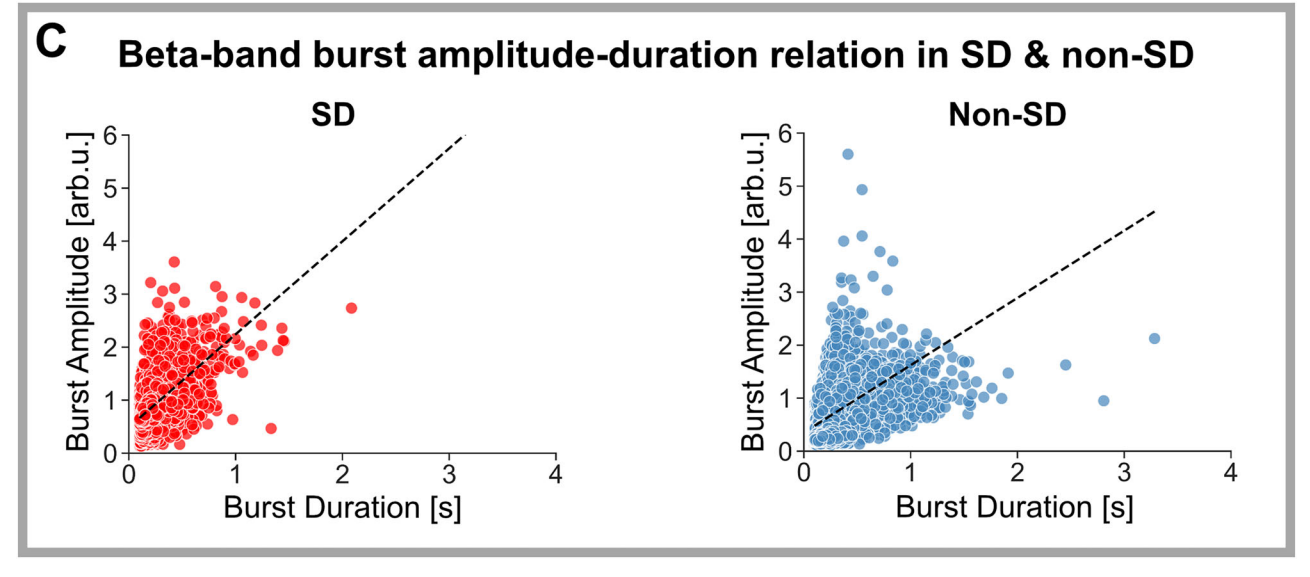
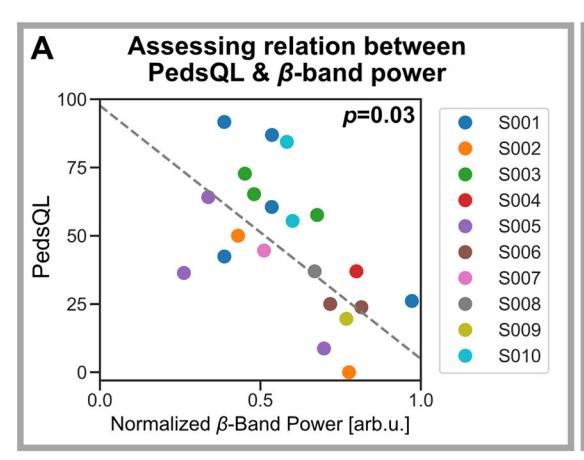


Fig. 3 | **Beta-band bursting activity during status dystonicus. A** Example betaband bursting activity (grey) shown for participant SO04 during SD. Bursts (shaded regions) were defined as activity greater than the 75th percentile (red dotted line) of beta envelope amplitude (black curve) and lasting >100 ms. **B** Across all participants and recordings, the mean burst amplitude (left panel) increased during SD (p < 0.001, n = 183), while there was no difference between SD and non-SD in the mean burst rate (central panel; p = 0.766, n = 183) and mean burst duration (right panel; p = 0.826, n = 183) using Mann-Whitney U-tests. **C** For each detected burst across all patients, burst amplitude was plotted against burst duration separately for SD (left panel) and non-SD (right panel). Using GLMMs, Burst amplitude was correlated to burst duration in both states (SD: β = 1.754; p < 0.001, non-SD:

 β = 1.270; p < 0.001). However, SD was further characterized by a stronger amplitude-duration relationship, with significantly higher amplitudes for a given duration (β = 0.484; p < 0.001) and higher baseline burst amplitude (adjusted intercept: β = 0.489 vs. β = 0.35; p < 0.001). For both burst plots, the relation between the burst amplitude and duration is shown as a black dotted line (using corresponding GLMM β -values for slope and intercept). In box plots, central marks indicated the median and edges the 25th and 75th percentiles of the distribution, and whiskers indicated minimal and maximal values per hemisphere. Arb.u. arbitrary units. GLMM, generalized linear mixed-effects model. SD, status dystonicus.
**p < 0.01. *p < 0.05.



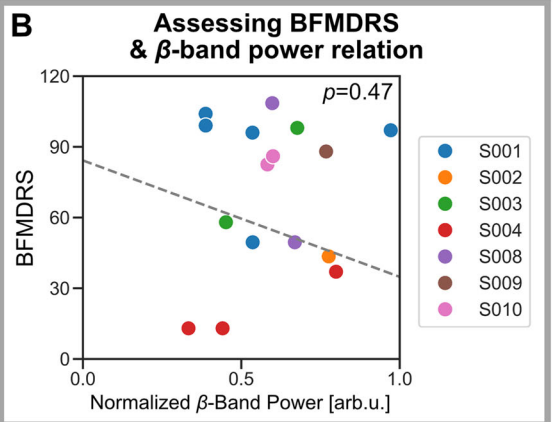


Fig. 4 | **GPi activity and correlation to clinical metrics.** A Lower health related quality of life (i.e. lower PedsQL) was significantly associated with higher beta-band power (p = 0.030; $\beta = -92.7$), using GLMMs computed with LFP and clinical metrics measured at multiple time points across all participants (participant color labels shown in legend). This association was not modified by dystonia state type (SD vs. non-SD; p = 0.746; $\beta = 14.9$) nor its interaction with beta-band power (p = 0.864; $\beta = -11.6$). **B** There were no significant correlations between band-limited powers

and BFMDRS using GLMMs, as shown for beta-band power (p = 0.474; $\beta = -49.4$). For each plot shown, the relation between the given band-limited power and clinical metric is shown as a grey dotted line (using corresponding GLMM β -values for slope and intercept), and the p-value of the correlation shown in the top right. Arb.u. arbitrary units, BFMDRS Burke-Fahn-Marsden Dystonia Rating Scale, GLMM generalized linear mixed-effects model, LFP local field potential, PedsQL Pediatric Quality of Life Inventory, SD status dystonicus.

using family-reported feedback. The PedsQL total score was determined at each assessment time.

LFP time series recordings and signal processing

Time series neural recordings. LFP time series recordings were acquired using the Percept PC device (250 Hz sampling rate). LFPs were labeled as occurring in 'SD'- or 'non-SD'- dystonicus based on clinical assessment. Recordings were conducted with DBS off via bipolar montage (i.e., signal subtraction) using BrainSense Streaming (Indefinite Streaming mode) from all three possible contact pairs simultaneously (0–2 or 1–3 and 0–3). No significant movement or electrocardiographic artifacts were observed in raw time series data traces, and beta-band filtered data using fourth-order zero-phase Butterworth bandpass filters and Hilbert envelopes were obtained for visualization (Fig. 1C). All recordings were filtered (Python SciPy butter function: high pass = 1 Hz, low pass = 100 Hz) and then converted to the frequency domain.

Power spectral density estimations. Power spectral density (PSD) was computed from each raw time series recording using Welch's method (Python SciPy welch function) with a Hann window of 1s, window-overlap of 500 ms, and a 256-point fast Fourier transform (FFT). For each participant, the channel with highest relative power during SD was selected in each hemisphere, and the single hemisphere with the most power was selected per participant as done in prior studies²⁰. To compare LFP recordings across time, dystonia state, and participants, PSDs were normalized by dividing by the total power, since absolute power varies with local tissue properties and electrode impedance. PSDs were used to assess power in various frequency bands, the periodic component of the LFP for peak analysis, and bursting activity.

Band-limited power analysis. Band-limited power was calculated as the total within each of the canonical frequency bands defined as theta (3-7 Hz), alpha (7-12.5 Hz) and beta (12.5-30 Hz), given the correlation of low-frequency and beta-band activity between hypo- and hyperkinetic dystonic symptoms in prior studies^{16,17,55}. The total power in each band was compared between SD and non-SD for each participant and across all participants. A generalized linear mixed-effects model (GLMM) was used to assess the isolated effect of dystonia state on band-limited beta-band power, controlling for intra-patient and interepisode variability. This was computed using dystonia state as a fixed

effect, participant as a random intercept, and the specific SD episode as a random slope nested within patients.

Periodic component analysis. To separate periodic and aperiodic activity in the LFPs, PSDs of each recordings were modeled using the Fitting Oscillations & One Over f (FOOOF) algorithm⁵¹. This approach models aperiodic activity using an aperiodic component, reflecting 1/ frequency- (1/f)-like characteristics, with a variable number of periodic components (putative oscillations) fitted with Gaussian models as peaks rising above the aperiodic component⁵¹. Background aperiodic activity was modeled using the power-law function, where the power is proportional to 1/f and decreases with f. The periodic peak center frequencies, bandwidths and powers over the aperiodic component were computed, without requiring predefining specific power bands of interest while controlling for the aperiodic component. The peak powers were compared between status and non-status for each participant and across all participants. A GLMM was used to assess the isolated effect of dystonia state on periodic power, using dystonia state as a fixed effect, participant as a random intercept, and the specific SD episode as a random slope nested within patients.

Periodic component associations with demographics, phenomenology and etiology. To evaluate the effects of dystonia state (SD vs non-SD), age, sex, phenomenology (tonic vs. phasic), and etiology (inherited vs. acquired) on beta-band periodic peak power, we computed individual GLMMs using each as a fixed effect separately. Random intercepts were used by each GLMM for each participant to account for within-subject variability. We then assessed the effect of concurrent sedating medications at the time of recording on peak power. Separate GLMMs were computed using exposure to either benzodiazepines, non-benzodiazepine sedating medications (clonidine, chloral hydrate or baclofen), or any sedating medications (benzodiazepine or non-benzodiazepine) in general as fixed effects. Lastly, a GLMM was computed using weight-based total daily benzodiazepine dosage as a fixed-effect, converted to Diazepam-equivalent dosing for non-Diazepam benzodiazepines (Supplementary Data 1). Each GLMM applied random coefficients for each patient's medication-power relation, and random intercepts for each patient. The p- and β -values of each fixed effect were computed. The statistical power of each GLMM was computed using a simulation-based power analysis (Supplementary Material).

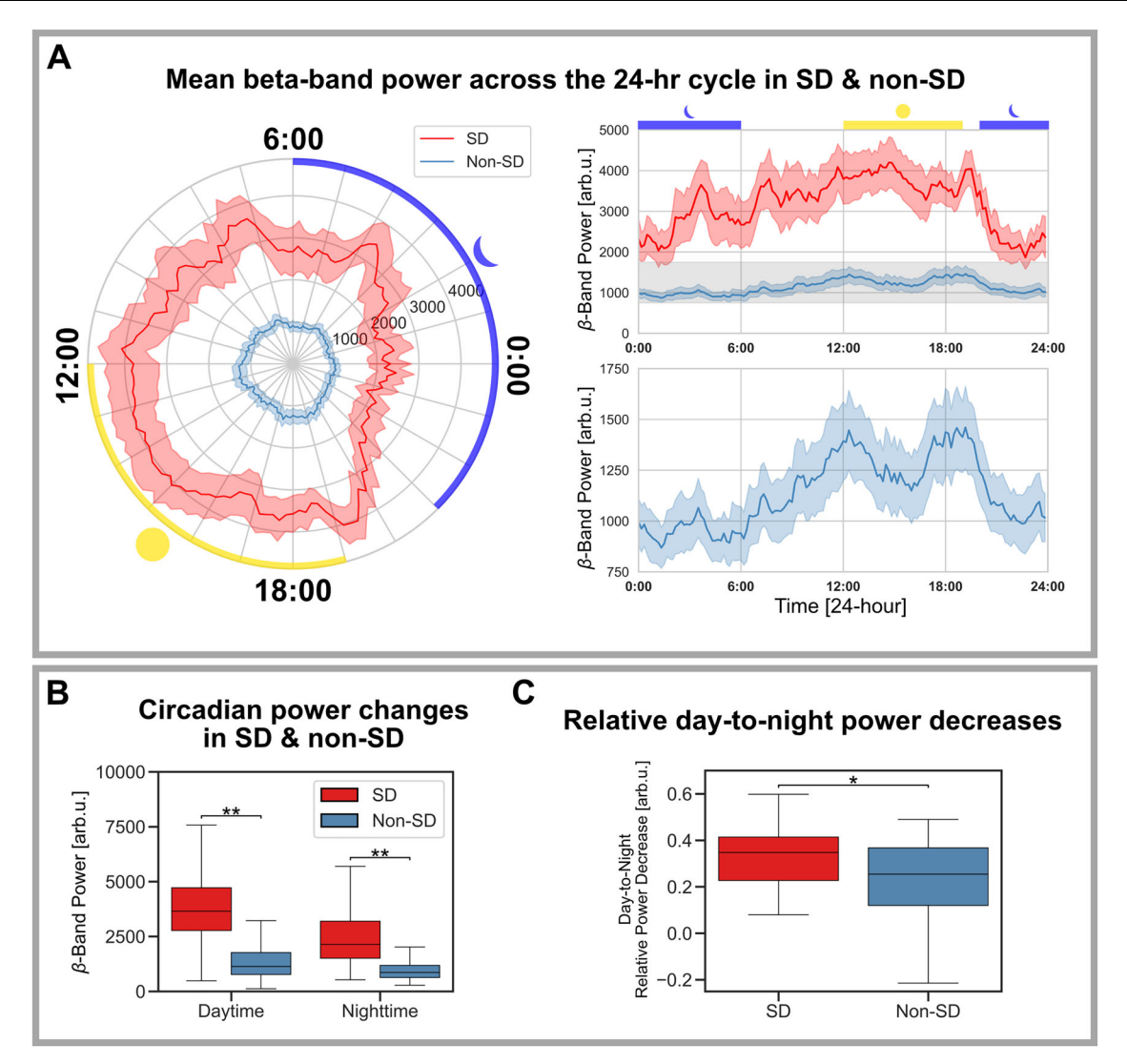


Fig. 5 | **Circadian periodicity and power dynamics in dystonia states.** All figure panels were constructed using data from participant S004. **A** GPi narrowband betaband activity was passively recorded longitudinally, with daytime defined as 12:00-19:00 (yellow regions, sun symbol) and nighttime as 21:00-06:00 (dark blue regions, moon symbol). Circular polar plots (left panel) showed beta-band power (radial axis) vs. time of day (angular axis), with the mean (lines) and 95% confidence interval (shaded regions) over a 24-h cycle shown for both SD and non-SD using 10-minutes averaged increments. Circadian beta-band power fluctuations in both SD and non-SD were compared using linear plots (right upper panel) with the 95% confidence intervals shown in shaded colors. Circadian fluctuations during the non-

SD period (grey region in right upper panel) were more evident when plotting separately (right lower panel). **B** The mean daytime ($p_{corrected} < 0.001$, n = 4115) and nighttime ($p_{corrected} < 0.001$, n = 5386) beta-band powers were significantly greater in SD (Mann-Whitney U-test, Bonferroni-corrected for multiple comparisons). **C** The proportional change in power from daytime to nighttime was greater in SD ($p_{corrected} = 0.007$, n = 9501; Mann-Whitney U-test). In box plots, central marks indicate the median and edges the 25th and 75th percentiles of the distribution, and whiskers indicate minimal and maximal values per hemisphere. Arb.u. arbitrary units. SD, status dystonicus. **p < 0.01. *p < 0.05.

Beta-band bursting. To assess bursting activity in the beta-band, peak frequency of the LFP periodic component was first computed using the FOOOF⁵¹ algorithm on each recording's PSD. Each LFP recording was *z*-score normalized²⁰, then bandpass filtered ±3 Hz around the predetermined beta peak frequency and envelopes determined using the Hilbert transform^{20,24–26,61}. Beta bursts were detected separately in each LFP recording using a threshold of 75th percentile of the beta envelope amplitude^{20,24–26,61}. The average burst duration and bursting rate, defined as the number of bursting episodes per minute, were determined for each recording (beta bursts <100 ms duration were excluded)^{25,26}. Beta burst amplitude was calculated as the maximum beta envelope amplitude during the beta burst. Bursting metrics were compared between SD and non-SD states.

Next, individual bursts were further analyzed by plotting burst amplitude vs. duration for all bursts, separately in SD and non-SD states²⁵. GLMMs (Python Statsmodels) were used to examine the relationship between burst duration and amplitude, controlling for group differences (SD vs non-SD) and accounting for random variability across individual bursts. The model included burst duration and dystonia state type (SD vs non-SD) as fixed effects, as well as their interaction to test whether the relationship between duration and amplitude differed between SD and non-SD. Random effects allowed for variability in burst-specific slopes and intercepts. Statistically significant factors were determined, and if significant the slopes and intercepts were then compared between SD and non-SD.

Aperiodic LFP component analysis. Based on the FOOOF method used to calculate separate periodic components of the LFPs, the aperiodic components were also extracted for each recording to analyze non-oscillatory background activity that has no characteristic

frequency⁵¹. First, the aperiodic offset, representing the positive or negative translation of the whole spectrum, was calculated. Next, the aperiodic exponent describes the negative slope of the 1/f-like activity. These two aperiodic features were then compared between SD and non-SD for all recordings individually for each participant (if both SD and non-SD recordings were present), as well as between SD and non-SD across all recordings from all participants. GLMMs were used to assess the isolated effect of dystonia state on aperiodic offset and exponent, respectively, each using dystonia state as a fixed effect, participant as a random intercept, and the specific SD episode as a random slope nested within patients.

Correlation between clinical and LFP metrics. GLMMs were used to assess the relation between clinical (PedsQL or BFMDRS) and LFP metrics (Python Lmer). Specifically, separate models were used for each clinical metric, with the clinical metric as the dependent variable. A GLMM was created using the band-limited beta-band power as the independent variable (fixed effects), and the effects of dystonia state type (either SD or non-SD) and the interaction of beta-band power and dystonia state as additional fixed effects and random intercepts for each participant. This interaction was included to assess if the effect of band-limited beta-band power on the clinical metric changes depending on the dystonia state.

Separate models were used to assess the relations between each clinical metric and band-limited alpha-band or theta-powers respectively, each model also including fixed effects of the dystonia state and the interaction of the model's respective band-limited power factor with dystonia state, again with random intercepts for each participant. Next, a GLMM was computed to assess the relation between BFMDRS and PedsQL, using BFMDRS, dystonia state and the BFMDRS-state interaction as fixed effects and participants as random intercepts. Lastly, all models were computed again separately using the average band-limited powers between the optimal contact in both hemispheres for each participant as fixed effects, instead of the band-limited power from the single optimal hemispheres. The p- and β -values of each fixed effect were computed, as well as the overall model R^2 if at least one factor showed significance.

Narrowband beta-band spectral amplitude recordings. Chronic LFP recordings were conducted using the BrainSense Timeline function at frequencies within the beta-band for the left hemisphere of one participant, S004. The hemisphere and center frequency were based on a BrainSense Survey conducted during the SD period, which provided to clinicians a PSD which demonstrated visually the peak frequency to select. The average LFP power within this clinician-selected frequency band of interest (center frequency ±2.5 Hz) over 10-minutes was recorded and stored every 10-minutes. The average power over the course of the recording duration for each 10-minute interval in the 24-hour cycle was calculated for SD and non-SD respectively. While stimulation remained turned on at the usual programmed settings (Supplementary Table 1), power at a center frequency of 15.63 Hz was recorded for the majority of the recording, except for the first few days at 12.7 Hz (March 23-27, 2023).

Circular statistics of beta-power dynamics in SD and non-SD. To assess the presence and characteristics of circadian modulation in beta-band power during SD and non-SD, the Rayleigh test was used to evaluate whether LFP power was non-uniformly distributed over 24 h (Python Scipy). To compare the overall distribution shapes between SD and non-SD, a permutation-based Kuiper test was used as a non-parametric circular analogue of the Kolmogorov–Smirnov test. The Kuiper V statistic was recalculated across 10,000 permutations of group labels to obtain an empirical *p*-value under the null hypothesis of distributional equivalence.

Circadian periodicity in beta-power dynamics in SD and non-SD. A Linear Autoregressive (LAR) model was used to study temporal dependencies and periodicity of the circadian power data for in SD and non-SD states. LAR models allow the prediction of time series data, using a linear combination of prior values (lags) to model the current value, as done in prior work by Provenza et al. studying circadian periodicity of narrowband LFP data³⁹. The LAR model was described as:

$$X_t = c + \phi_1 X_{t-1} + \phi_2 X_{t-2} + \dots + \phi_p X_{t-p} + \varepsilon_t$$
 (1)

where X_t is the value of the narrowband power at time t, c is a constant term, ϕ_p is the linear multiplier for p^{th} lag's power-value X_{t-p} , and ε_t is the error term.

Time series data were transformed into a format for supervised learning by creating up to 144 lagged features, since each 24-hour cycle has 144 timepoints separated by 10-minutes (from X_{t-1} to X_{t-144}). Significant lagged features were selected through iterative five-fold cross-validation to prevent overfitting. At each iteration, an Ordinary Least Squares (OLS) regression model was trained, and lags with p-values < 0.05 in at least 3 of the 5 folds were retained. The final model was then trained on the full dataset using the selected lags, producing an optimized regression equation. Model performance was evaluated using five-fold cross-validation, and R^2 (proportion of variance explained by the model) was computed for each fold and averaged. This approach ensured the inclusion of only robust, statistically significant lagged predictors while minimizing overfitting and providing a reliable measure of predictive accuracy. Finally, the R^2 and significant lags were compared between SD and non-SD.

Next, we repeated this but calculated the R^2 values on a daily basis and statistically compared the mean daily R^2 between SD and non-SD to assess for differences in the level of fit in LAR.

Beta-band power changes between daytime and nighttime in SD and non-SD. The average narrowband beta-band power during daytime (defined as 12:00 – 19:00) was compared to nighttime (21:00 – 06:00) during either SD or non-SD states. A slightly larger duration of daytime and nighttime was chosen than in prior literature³⁷. Late mornings (06:00–12:00) were not analyzed similar to prior studies³⁷, as transition between sleep and wake may vary on a day-to-day basis. The average daytime and nighttime powers were compared in SD and non-SD, respectively. The average proportional change between daytime and nighttime power in a 24-hour cycle across all days was then compared between SD and non-SD.

Binary dystonia-state machine learning classifiers. Random forest classifiers (Python Scikit-learn) were trained to classify LFP PSD-data as belonging to SD or non-SD state⁷¹. SD-state was used as the label, and the powers at each frequency in the filtered PSD were used as model features. To prevent data leakage and test model robustness on unseen data, LOPOCV was used where the model was trained and tested ten separate folds. In each fold, a model was trained using nine patients' recording data and tested on a holdout tenth patient's data. This was repeated for a total of ten folds, and a cumulative confusion matrix from adding the confusion matrices of each fold was calculated, and corresponding performance metrics including cumulative AUROC, precision and recall were computed⁷¹.

This was repeated, but instead using LOOCV, where in each fold the model was trained on *n*-1 recordings across all patients and tested on a single holdout recording. This was repeated *n* times, and cumulative confusion matrices and performance metrics were calculated.

Statistics. Shapiro's normality test was performed on all data, including band-limited powers, periodic peak power, and beta-band bursting metrics (amplitude, burst rate), to determine the appropriate statistical tests. If the test statistics concluded that data was not normally

distributed (p > 0.05), non-parametric tests were performed. Specifically, the Mann-Whitney U-test was used for all comparisons of means between SD and non-SD for each LFP metric. Otherwise, Welch's t-test was used. The Bonferroni correction was used for multiple comparisons. All results are indicated as mea $n \pm$ standard deviation and reported as significant at an α level of 0.05.

Reporting summary

Further information on research design is available in the Nature Portfolio Reporting Summary linked to this article.

Data availability

The data generated in this study, including the source data of all figures, are provided in the Source Data file. Source data are provided with this paper.

Code availability

All code is publicly available on GitHub (https://github.com/arjunastra/SD manuscript codes).

References

- Albanese, A. et al. Phenomenology and classification of dystonia: A consensus update. Mov. Disord. 28, 863–873 (2013).
- Goswami, J. N., Roy, S. & Patnaik, S. K. Pediatric Dystonic Storm: A Hospital-Based Study. Neurol.: Clin. Pract. 11, e645 (2021).
- Saini, A. G. et al. Status Dystonicus in Children: A Cross-Sectional Study and Review of Literature. J. Child Neurol. 37, 441–450 (2022).
- Meijer, I. A. & Fasano, A. Status Dystonicus. in Movement Disorder Emergencies: Diagnosis and Treatment (ed. Frucht, S. J.) 183–199 (Springer International Publishing, Cham, 2022), https://doi.org/10. 1007/978-3-030-75898-1 10.
- Vogt, L. M. et al. Recommendations for the Management of Initial and Refractory Pediatric Status Dystonicus. Mov. Disord. 39, 1435–1445 (2024).
- Ruiz-Lopez, M. & Fasano, A. Rethinking status dystonicus. Mov. Disord. 32, 1667–1676 (2017).
- Allen, N. M., Lin, J.-P., Lynch, T. & King, M. D. Status dystonicus: a practice guide. Developmental Med. Child Neurol. 56, 105–112 (2014).
- Vogt, L. M. et al. Deep Brain Stimulation for Refractory Status Dystonicus in Children: Multicenter Case Series and Systematic Review. Ann. Neurol. 95, 156–173 (2024).
- Benato, A. et al. Long-term effect of subthalamic and pallidal deep brain stimulation for status dystonicus in children with methylmalonic acidemia and GNAO1 mutation. J. Neural Transm. (Vienna) 126, 739–757 (2019).
- Ben-Haim, S. et al. Deep brain stimulation for status dystonicus: a case series and review of the literature. Stereotact. Funct. Neurosurg. 94, 207–215 (2016).
- Lobato-Polo, J. et al. Deep brain stimulation surgery for status dystonicus: a single-center experience and literature review. World Neurosurg. 114, e992–e1001 (2018).
- Simonyan, K., Cho, H., Hamzehei Sichani, A., Rubien-Thomas, E. & Hallett, M. The direct basal ganglia pathway is hyperfunctional in focal dystonia. *Brain* 140, 3179–3190 (2017).
- 13. Tisch, S. & Limousin, P. Neurophysiological insights in dystonia and its response to deep brain stimulation treatment. *Exp. Brain Res* **238**, 1645–1657 (2020).
- Quartarone, A. & Hallett, M. Emerging concepts in the physiological basis of dystonia. Mov. Disord. 28, 958–967 (2013).
- Lofredi, R. et al. Striato-pallidal oscillatory connectivity correlates with symptom severity in dystonia patients. *Nat. Commun.* 15, 8475 (2024).
- Scheller, U. et al. Pallidal low-frequency activity in dystonia after cessation of long-term deep brain stimulation. Mov. Disord. 34, 1734–1739 (2019).

- Neumann, W.-J. et al. A localized pallidal physiomarker in cervical dystonia. Ann. Neurol. 82, 912–924 (2017).
- Neumann, W.-J. et al. Enhanced low-frequency oscillatory activity of the subthalamic nucleus in a patient with dystonia. *Mov. Disord.* 27, 1063–1066 (2012).
- Geng, X. et al. Comparison of oscillatory activity in subthalamic nucleus in Parkinson's disease and dystonia. *Neurobiol. Dis.* 98, 100–107 (2017).
- 20. Lofredi, R. et al. Pallidal beta bursts in Parkinson's disease and dystonia. *Mov. Disord.* **34**, 420–424 (2019).
- Little, S. & Brown, P. What brain signals are suitable for feedback control of deep brain stimulation in Parkinson's disease? *Ann. N. Y. Acad. Sci.* 1265, 9–24 (2012).
- Neumann, W.-J. et al. Subthalamic synchronized oscillatory activity correlates with motor impairment in patients with Parkinson's disease. Mov. Disord. 31, 1748–1751 (2016).
- 23. Tinkhauser, G. et al. Beta burst coupling across the motor circuit in Parkinson's disease. *Neurobiol. Dis.* **117**, 217–225 (2018).
- Piña-Fuentes, D. et al. The characteristics of pallidal low-frequency and beta bursts could help implementing adaptive brain stimulation in the parkinsonian and dystonic internal globus pallidus. Neurobiol. Dis. 121, 47–57 (2019).
- Tinkhauser, G. et al. Beta burst dynamics in Parkinson's disease OFF and ON dopaminergic medication. *Brain* 140, 2968–2981 (2017).
- Yu, Y. et al. Parkinsonism alters beta burst dynamics across the basal ganglia-motor cortical network. J. Neurosci. 41, 2274 (2021).
- Lofredi, R. et al. Subthalamic beta bursts correlate with dopaminedependent motor symptoms in 106 Parkinson's patients. npj Parkinsons Dis. 9, 1–9 (2023).
- Darmani, G. et al. Long-term recording of subthalamic aperiodic activities and beta bursts in Parkinson's Disease. Mov. Disord. 38, 232–243 (2023).
- Gao, R., Peterson, E. J. & Voytek, B. Inferring synaptic excitation/ inhibition balance from field potentials. *NeuroImage* 158, 70–78 (2017)
- 30. Manning, J. R., Jacobs, J., Fried, I. & Kahana, M. J. Broadband shifts in local field potential power spectra are correlated with single-neuron spiking in humans. *J. Neurosci.* **29**, 13613–13620 (2009).
- Voytek, B. & Knight, R. T. Dynamic network communication as a unifying neural basis for cognition, development, aging, and disease. *Biol. Psychiatry* 77, 1089–1097 (2015).
- 32. Wiest, C. et al. Subthalamic Nucleus Stimulation-Induced Local Field Potential Changes in Dystonia. *Mov. Disord.* **38**, 423–434 (2023).
- 33. Iodice, A. & Pisani, F. Status dystonicus: management and prevention in children at high risk. *Acta Biomed.* **90**, 207–212 (2019).
- 34. Yin, Z. et al. Pallidal activities during sleep and sleep decoding in dystonia, Huntington's, and Parkinson's disease. *Neurobiol. Dis.* **182**, 106143 (2023).
- 35. Yin, Z. et al. Generalized sleep decoding with basal ganglia signals in multiple movement disorders. npj Digit. Med. 7, 1–13 (2024).
- Anjum, M. F. et al. Multi-night cortico-basal recordings reveal mechanisms of NREM slow-wave suppression and spontaneous awakenings in Parkinson's disease. *Nat. Commun.* 15, 1793 (2024).
- 37. Cagle, J. N. et al. Chronic intracranial recordings in the globus pallidus reveal circadian rhythms in Parkinson's disease. *Nat. Commun.* **15**, 4602 (2024).
- 38. Baud, M. O. et al. Multi-day rhythms modulate seizure risk in epilepsy. *Nat. Commun.* **9**, 88 (2018).
- Provenza, N. R. et al. Disruption of neural periodicity predicts clinical response after deep brain stimulation for obsessive-compulsive disorder. *Nat. Med.* 30, 3004–3014 (2024).
- Neumann, W.-J., Gilron, R., Little, S. & Tinkhauser, G. Adaptive Deep Brain Stimulation: From Experimental Evidence Toward Practical Implementation. Mov. Disord. 38, 937–948 (2023).

- Balachandar, A., Phokaewvarangkul, O. & Fasano, A. Closed-loop systems for deep brain stimulation to treat neuropsychiatric disorders. Expert Review of Medical Devices 0, 1–12.
- Phokaewvarangkul, O., Balachandar, A. & Fasano, A. Chapter 17 -Closed-loop systems. in *Handbook of Digital Technologies in Movement Disorders* (eds. Bhidayasiri, R. & Maetzler, W.) 269–284 (Academic Press, 2024), https://doi.org/10.1016/B978-0-323-99494-1.00002-2.
- Gilron, R. et al. Sleep-Aware Adaptive Deep Brain Stimulation Control: Chronic Use at Home With Dual Independent Linear Discriminate Detectors. Front. Neurosci. 15, (2021).
- Smyth, C. et al. Adaptive Deep Brain Stimulation for sleep stage targeting in Parkinson's disease. Brain Stimulation: Basic, Transl., Clin. Res.F Neuromodulation 16, 1292–1296 (2023).
- Yan, H. et al. The Child & Youth CompreHensive Longitudinal Database for Deep Brain Stimulation (CHILD-DBS). Childs Nerv. Syst. 37, 607–615 (2021).
- 46. Horn, A. et al. Lead-DBS v2: Towards a comprehensive pipeline for deep brain stimulation imaging. *Neuroimage* **184**, 293–316 (2019).
- 47. Yokochi, F. et al. Resting-State Pallidal-Cortical Oscillatory Couplings in Patients With Predominant Phasic and Tonic Dystonia. *Front. Neurol.* **9**, (2018).
- 48. Fasano, A. et al. Status dystonicus: Predictors of outcome and progression patterns of underlying disease. *Mov. Disord.* **27**, 783–788 (2012).
- 49. Burke, R. E. et al. Validity and reliability of a rating scale for the primary torsion dystonias. *Neurology* **35**, 73–77 (1985).
- Pintér, D., Janszky, J. & Kovács, N. Minimal Clinically Important Differences for Burke-Fahn-Marsden Dystonia Rating Scale and 36-Item Short-Form Health Survey. Mov. Disord. 35, 1218–1223 (2020).
- Donoghue, T. et al. Parameterizing neural power spectra into periodic and aperiodic components. *Nat. Neurosci.* 23, 1655–1665 (2020).
- Desai, A. D. et al. Validity and Responsiveness of the Pediatric Quality of Life Inventory (PedsQL) 4.0 Generic Core Scales in the Pediatric Inpatient Setting. JAMA Pediatrics 168, 1114–1121 (2014).
- Varni, J. W., Seid, M. & Kurtin, P. S. PedsQL 4.0: reliability and validity of the Pediatric Quality of Life Inventory version 4.0 generic core scales in healthy and patient populations. *Med Care* 39, 800–812 (2001).
- 54. Varni, J. W., Limbers, C. A. & Burwinkle, T. M. Impaired health-related quality of life in children and adolescents with chronic conditions: a comparative analysis of 10 disease clusters and 33 disease categories/severities utilizing the PedsQL™ 4.0 Generic Core Scales. *Health Qual. Life Outcomes* **5**, 43 (2007).
- Lofredi, R. et al. Pallidal Beta Activity Is Linked to Stimulation-Induced Slowness in Dystonia. Mov. Disord. 38, 894–899 (2023).
- Alamri, A. et al. Deep Brain Stimulation of the Globus Pallidus Internus in a Child with Refractory Dystonia due to L2-Hydroxyglutaric Aciduria. Stereotact. Funct. Neurosurg. 102, 209–216 (2024).
- 57. Fasano, A. et al. Local Field Potential-Based Programming: A Proofof-Concept Pilot Study. *Neuromodulation: Technology at the Neural Interface* **n/a**, (2021).
- Tinkhauser, G. et al. The modulatory effect of adaptive deep brain stimulation on beta bursts in Parkinson's disease. *Brain* 140, 1053–1067 (2017).
- Brittain, J.-S. & Brown, P. Oscillations and the basal ganglia: Motor control and beyond. *NeuroImage* 85, 637–647 (2014).
- Weinberger, M. & Dostrovsky, J. O. A basis for the pathological oscillations in basal ganglia: the crucial role of dopamine. *Neu*roReport 22, 151 (2011).
- Wang, D. D. et al. Pallidal Deep-Brain Stimulation Disrupts Pallidal Beta Oscillations and Coherence with Primary Motor Cortex in Parkinson's Disease. J. Neurosci. 38, 4556–4568 (2018).

- Mink, J. W. Special concerns in defining, studying, and treating dystonia in children. Mov. Disord. 28, 921–925 (2013).
- 63. Gorodetsky, C. & Fasano, A. Approach to the Treatment of Pediatric Dystonia. *Dystonia* 1, 10287 (2022).
- 64. Gimeno, H. et al. Evaluation of functional goal outcomes using the Canadian Occupational Performance Measure (COPM) following Deep Brain Stimulation (DBS) in childhood dystonia. *Eur. J. Paediatr. Neurol.* **18**, 308–316 (2014).
- Gimeno, H., Gordon, A., Tustin, K. & Lin, J.-P. Functional priorities in daily life for children and young people with dystonic movement disorders and their families. *Eur. J. Paediatr. Neurol.* 17, 161–168 (2013).
- Gimeno, H., Tustin, K., Selway, R. & Lin, J.-P. Beyond the Burke–Fahn–Marsden Dystonia Rating Scale: Deep brain stimulation in childhood secondary dystonia. *Eur. J. Paediatr. Neurol.* 16, 501–508 (2012).
- 67. Kuiper, M. J. et al. The Burke-Fahn-Marsden Dystonia Rating Scale is Age-Dependent in Healthy Children. *Mov. Disord. Clin. Pract.* **3**, 580–586 (2016).
- 68. Wiest, C. et al. The aperiodic exponent of subthalamic field potentials reflects excitation/inhibition balance in Parkinsonism. *eLife* **12**, e82467 (2023).
- Gilron, R. et al. Long-term wireless streaming of neural recordings for circuit discovery and adaptive stimulation in individuals with Parkinson's disease. Nat. Biotechnol. 39, 1078–1085 (2021).
- 70. Al Azri, N. et al. Status Dystonicus in Children: Is it more Common than we Realize? *Mov Disord Clin Pract* (2025). https://doi.org/10. 1002/mdc3.70131.
- 71. Pedregosa, F. et al. Scikit-learn: Machine Learning in Python. J. Mach. Learn. Res. 12, 2825–2830 (2011).

Acknowledgements

Dr. George Ibrahim is the Abe Bresver Chair in Functional Neurosurgery and received a Garry Hurvitz Centre for Brain and Mental Health Program Development Grant to support this work. Dr. Arjun Balachandar received the Parkinson Canada Clinician Scientist Research Fellowship to support his research work. We thank all participants and their families who participated in this study. Without their dedication to contribute to the understanding and treatment of dystonia, our research would not be possible.

Author contributions

A.B. contributed to organization and execution of the research project, designed and executed the statistical analyses, and wrote all drafts of the manuscript. L.M.V. contributed to the execution of the research project, reviewed and critiqued the statistical analyses, conducted clinical assessments of all participants, and co-wrote the manuscript. K.M., S.C.C., M.E., A.L.M., and S.B. contributed to the review and critique of the statistical analyses and manuscript. A.F. contributed to the organization of the research project and the review and critique of the manuscript. C.G. conceived, organized, and executed the research project, designed the statistical analyses, reviewed and critiqued the statistical analyses, conducted clinical assessments of all participants, and obtained the intracranial recordings. G.I. conceived, organized, and executed the research project, designed the statistical analyses, reviewed and critiqued the statistical analyses, and performed the surgeries. All authors provided input and substantial revisions to the manuscript.

Competing interests

C.G. reports consultancies for Medtronic and Ipsen, advisory board membership for Medtronic. A.F. reports consultancies for AbbVie, Medtronic, Boston Scientific, Iota, Inbrain, Inbrain Pharma, and Ceregate; advisory board membership for AbbVie and Boston Scientific; honoraria from AbbVie, Medtronic, Boston Scientific, Sunovion, Ipsen, and Merz; and royalties from Springer. He has also received grants from

the University of Toronto, Weston Foundation, Abbvie, Medtronic, Boston Scientific, and CIHR. G.I.M reports consultancies for Synergia Inc., Medtronic Inc., and LivaNova Inc.; advisory board membership for Synergia Inc.; royalties from Springer; grants from LivaNova Inc.; and speaking fees from Medtronic Inc. and LivaNova Inc. All personal fees are not linked to the here presented study results. The remaining authors declare no competing interests.

Additional information

Supplementary information The online version contains supplementary material available at https://doi.org/10.1038/s41467-025-64416-9.

Correspondence and requests for materials should be addressed to Carolina Gorodetsky or George M. Ibrahim.

Peer review information *Nature Communications* thanks Philippe De Vloo, who co-reviewed with Sara Smeets, Roxanne Lofredi and the other, anonymous, reviewer(s) for their contribution to the peer review of this work. A peer review file is available.

Reprints and permissions information is available at http://www.nature.com/reprints

Publisher's note Springer Nature remains neutral with regard to jurisdictional claims in published maps and institutional affiliations.

Open Access This article is licensed under a Creative Commons Attribution-NonCommercial-NoDerivatives 4.0 International License, which permits any non-commercial use, sharing, distribution and reproduction in any medium or format, as long as you give appropriate credit to the original author(s) and the source, provide a link to the Creative Commons licence, and indicate if you modified the licensed material. You do not have permission under this licence to share adapted material derived from this article or parts of it. The images or other third party material in this article are included in the article's Creative Commons licence, unless indicated otherwise in a credit line to the material. If material is not included in the article's Creative Commons licence and your intended use is not permitted by statutory regulation or exceeds the permitted use, you will need to obtain permission directly from the copyright holder. To view a copy of this licence, visit https://creativecommons.org/licenses/by-nc-nd/4.0/.

© The Author(s) 2025